



This is a repository copy of *Finite element assessment of the temperature field couple under joule heat and friction heat between a third rail and collector shoe*.

White Rose Research Online URL for this paper:

<http://eprints.whiterose.ac.uk/92563/>

Version: Accepted Version

Article:

Dong, L., Lewis, R., Li, C.X. et al. (2 more authors) (2015) Finite element assessment of the temperature field couple under joule heat and friction heat between a third rail and collector shoe. *Journal Of Engineering Tribology* , 229 (9). 1086 - 1094. ISSN 13506501

<https://doi.org/10.1177/1350650115573974>

Reuse

Unless indicated otherwise, fulltext items are protected by copyright with all rights reserved. The copyright exception in section 29 of the Copyright, Designs and Patents Act 1988 allows the making of a single copy solely for the purpose of non-commercial research or private study within the limits of fair dealing. The publisher or other rights-holder may allow further reproduction and re-use of this version - refer to the White Rose Research Online record for this item. Where records identify the publisher as the copyright holder, users can verify any specific terms of use on the publisher's website.

Takedown

If you consider content in White Rose Research Online to be in breach of UK law, please notify us by emailing eprints@whiterose.ac.uk including the URL of the record and the reason for the withdrawal request.

Finite element assessment of the temperature field couple under joule heat and friction heat between a third rail and collector shoe

Lin Dong¹, Roger Lewis^{2*}, Chuan Xi Li¹, Wei Bing Zhu¹ and He Shun Wang¹

¹School of Mechanical Engineering and Automation, Xihua University, Chengdu 610039, People's Republic of China

²Department of Mechanical Engineering, The University of Sheffield, Mappin Street, Sheffield S1 3JD, UK

*Corresponding author: Department of Mechanical Engineering, the University of Sheffield, Mappin Street, Sheffield S1 3JD, UK. email: roger.lewis@sheffield.ac.uk

Abstract: Based on the finite element software COMSOL Multiphysics 4.3b, a temperature field model for an aluminium/stainless steel composite third rail and a copper impregnated carbon collector shoe contact with coupling of joule heat and friction heat was established. A method of coupling the two kinds of heat was developed, the temperature fields were calculated, and the maximum coupled temperature change under different electric current, normal forces, sliding velocities and distances were studied. The results show that: the temperature distribution expands around the contact area in a descending tendency at positions closer to the electric contact area and the temperature gradients are higher; the maximum coupled temperature increases with an increase of electric current; with an increase of normal force, the maximum coupled temperature initially decreases then increases; the maximum coupled temperature increases initially then gradually becomes stable with an increase of sliding distance; an optimal normal force range exists in frictional sliding with an electric current, at which the maximum coupled temperature is at its lowest; joule heat and friction heat are competitive with each other. When normal force is lower, the joule heat becomes the main heat source, but when normal force is greater, mechanical friction heat becomes the main heat source.

Key Words: friction heat, joule heat, temperature field couple, finite element assessment

1 INTRODUCTION

The friction heat, joule heat and arc heat are the three main kinds of heat source in the frictional process for contacting sliding machine elements with an electric current passing through them [1, 2]. Joule heat is the process by which the passage of an electric current through a conductor releases heat. Arc heat is heating of a material by the heat energy from an electric arc. In relative sliding of a friction pair without current, the mechanical friction power which occurs in the process is converted to friction heat mostly. With repeated relative sliding and power conversion, the surface temperature of the friction pair is raised [3, 4]. In addition to the friction heat, joule heat and arc heat occurs between the friction pairs with electric current passing through. The continuous friction between asperities of the frictional pair makes the local temperature rise, and the rise will be intensified with the coupling of joule heat and arc heat [5-8]. The temperature rise resulting from the heat coupling may result in the friction pair material softening, and contact state changing, which can lead to wear loss increasing [8, 9].

The contact points of a current-carrying friction pair interface change constantly and therefore the temperature is difficult to measure accurately in the field and under experimental conditions. Until now, research reports of the temperature fields coupled in current-carrying tribological contacts are relatively rare, especially the assessment of friction heat and joule heat coupling. But the research is very important for industry applications and in particular

subway transportation, so that the temperature rise can be controlled in order to decrease the wear loss of materials.

In this paper, a sliding friction model under electric current was established using COMSOL Multiphysics 4.3b, of a composite conductor rail and a collector shoe used in a subway third rail traction system. Arc heat occurs when collector shoe and third rail lose or remake contact briefly. In this condition, the normal force between contact points is zero temporarily and the electrical contact points on the collector shoe and third rail are instantly offline. Because the arc heat is very high and not stable, it cannot be calculated by the finite element method. In the finite element simulation hypotheses, it is assumed that each electrical contact point is not in an offline case and the arc heat is ignored. The method of coupling the joule heat and friction heat was developed and the coupled temperature changing properties of the contact zone were revealed. The maximum coupled temperature change under different electric currents, normal forces, sliding velocities and sliding distances were studied.

2 FINITE ELEMENT ASSESSMENT

2.1 Third rail sliding contact model

Third rail traction systems use a conductor rail to transmit electrical power to a train in a subway. Figure 1 shows a schematic illustration of a third rail traction system. The aluminum/stainless steel composite conductive rail is a rolled thin strip of stainless steel around the top of an extruded aluminum body [10]. The conductive third rail is parallel to the two running rails and mounted on an insulator. The collector shoe slides on the top of the third rail and current is collected by the train through a collector shoe.

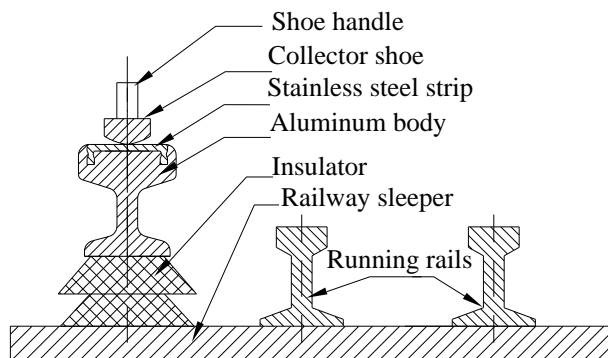


Fig. 1 Schematic illustration of a third rail traction system with a aluminum/stainless steel composite conductor rail and collector shoe

2.2 Finite element modelling and basic hypothesis

2.2.1 Meshed model

In the research, a sliding friction contact model was established as shown in Figure 2(a) by COMSOL Multiphysics 4.3b, based on a friction pair of an aluminum/stainless steel composite conductive rail and a copper impregnated carbon collector shoe Figure 2(b). A normal force F_n was applied on the top of collector shoe along the central line evenly, with a

relative sliding velocity V along the third rail longitudinal direction [5, 8]. An electric current I was passed through the collector shoe and composite conductor rail.

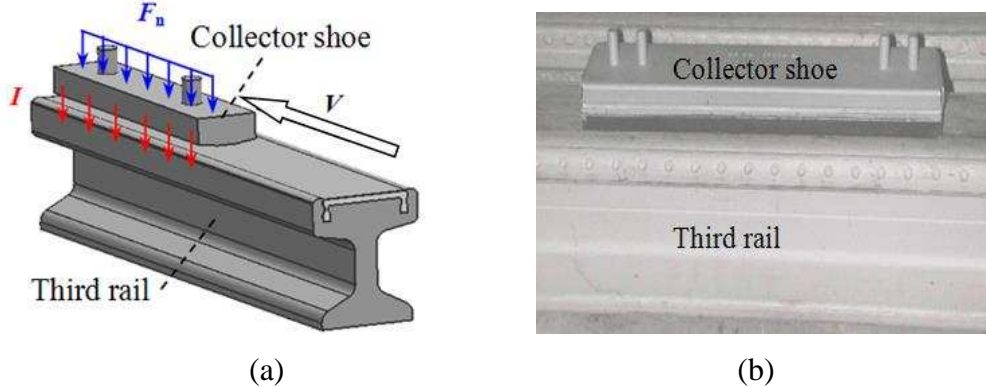


Fig. 2 (a) Conductor rail and collector shoe 3-D model; (b) Actual shoe and rail; (the white arrow means the collector shoe sliding direction)

In the finite element calculation, a 3-D model of the aluminium/stainless steel composite conductor rail and copper impregnated carbon collector shoe was established, as shown in Figure 3.

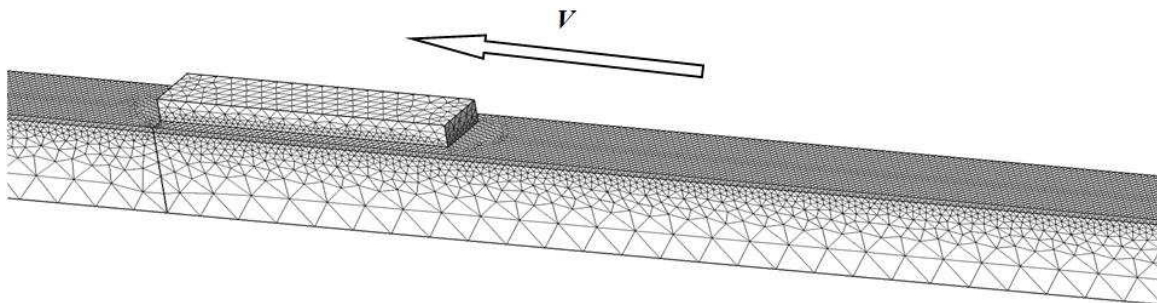


Fig. 3 Meshed 3-D model (the white arrow means the collector shoe sliding direction)

The geometric dimensions and materials were as follows: the upper sample was made of copper impregnated carbon material 270 mm long, 60 mm wide and 27 mm high; the middle sample was made of stainless steel material 6600 mm long, 92 mm wide and 6 mm high, and the lower sample which was made of aluminium material 6600 mm long, 92 mm wide and 100 mm high. The middle sample (stainless steel) forms a union with the lower sample (aluminium), which models the aluminium/stainless steel composite conductor rail. The union is kind of Boolean operation, which makes the FE “object” into a composite geometric component. The type of the finite elements is non-linear shape function. Total degrees of freedom are 2211076, the degrees of freedom of electric potential are 1054725, and the degrees of freedom of temperature are 1156351.

A joule heating module was used for thermal coupling in COMSOL Multiphysics 4.3b. A free tetrahedron mesh was used. For the relative motion, a moving coordinate system was applied, which was fixed at the central axis of the collector shoe. Then the relative friction movement between the third rail and collector shoe is realized.

The joule heat entered into the upper sample (collector shoe), middle sample and lower sample (aluminium/stainless steel composite conductor rail) in the form of a heat flux, and

was coupled by the sliding friction heat at the contact interfaces. In order to make the problem manageable and meaningful, the hypotheses were as follows:

- (a) Material parameters for each layer were isotropic;
- (b) Heat loss caused by radiation was ignored;
- (c) Power loss caused by eddy currents was ignored;
- (d) Heat carried away by abrasive debris was ignored;
- (e) Density and conductivity of the samples changes with temperature were ignored;
- (f) Surface membrane resistance between the friction pair was ignored;
- (g) Electrical contact of the friction pair was continuous and arcs did not occur.

Based on the hypotheses above and the principle of conservation of energy, transient heat transfer may be expressed as follows [11]:

$$\rho C_p \frac{\partial T}{\partial t} + \rho C_p \cdot V \cdot \nabla T = Q + \nabla \cdot (k \nabla T) \quad (1)$$

where, ρ is material density ($\text{kg} \cdot \text{m}^{-3}$); C_p is specific heat ($\text{J} \cdot \text{kg}^{-1} \cdot ^\circ\text{C}^{-1}$); T is node temperature ($^\circ\text{C}$); t is the relative sliding time (s); V is relative sliding velocity (m/h); Q is power produced by heat (W) and k is thermal conductivity ($\text{W} \cdot \text{m}^{-1} \cdot ^\circ\text{C}^{-1}$).

2.2.2 Boundary conditions

All of the degrees of freedom were constrained for the middle and lower sample, and normal force was applied to the top surface of the upper sample. The initial temperature T_0 of the model was set to room temperature that is 20°C . The boundary condition for the contact area was as follows [11]:

$$-r \cdot (-k \nabla T) = \dot{Q}_f + \dot{Q}_j \quad (2)$$

where k is thermal conductivity of material ($\text{W} \cdot \text{m}^{-1} \cdot ^\circ\text{C}^{-1}$); \dot{Q}_f is friction heat flux ($\text{W} \cdot \text{m}^{-2}$); \dot{Q}_j is Joule heat flux ($\text{W} \cdot \text{m}^{-2}$); r is outer normal direction of the object boundary and T is temperature.

2.2.3 Calculation of friction heat

In the process of relative sliding, friction heat passes into the contact friction pair in the form of heat flux. As for an area-area friction pair, the mechanical friction heat can be calculated by the equation as follows [2]:

$$Q_f = E_{cf} \mu F_n l \quad (J) \quad (3)$$

where E_{cf} is the energy conversion factor; μ is friction coefficient; F_n is normal force (N) and l is relative sliding distance of the friction pair (m). Then the friction heat flux can be calculated as below [2]:

$$\dot{Q}_f = \frac{E_{cf} \mu F_n V}{A_f} \quad (\text{W} \cdot \text{m}^{-2}) \quad (4)$$

where A_f is real contact area (m^2) and V is relative sliding velocity (m/s).

2.2.4 Calculation of joule heat

In the process of the assessment, the total joule heat can be calculated as the equation below [2]:

$$Q_j = I^2 R_c t \quad (\text{J}) \quad (5)$$

where I is electric current; R_c is the contact resistance and t is the relative sliding time (s). Then the contact resistance heat flux can be calculated as below [12]:

$$\dot{Q}_j = \frac{I^2 R_c}{A_c} \quad (\text{W} \cdot \text{m}^{-2}) \quad (6)$$

where A_c is total electrical contact area (m^2).

The physical essence of the contact resistance is the total of metal contraction resistance which caused by the contraction effect of the conductive spots when electric current is passing through the contacting surface. The electric contact resistance was calculated as follows [12]:

$$R_c = R_{c1} + R_{c2} = \frac{R_1}{4\alpha} + \frac{R_2}{4\alpha} \quad (\Omega) \quad (7)$$

where, R_{c1} is the contraction resistance of the collector shoe (Ω); R_{c2} is the contraction resistance of the third rail contact surface (Ω); α is the radius of the actual contact surface (m); R_1 is the resistance of collector shoe (Ω) and R_2 is the resistivity of the third rail contact surface (Ω).

2.2.5 Calculation of electrical contact area

The actual contact areas, through which the electric current passes and contracts, have a limited size. The following equation is used to calculate the total electric contact area [12]:

$$A_c = n A_s = \frac{F_n}{\xi H} \quad (\text{m}^2) \quad (8)$$

where A_s is the area of a single contact point (m^2); F_n is normal force (N); n is the number of single contact points; ξ is a correction factor and H is hardness (MPa). The radius of single contact point can be calculated while a single contact point was set to be round. Then the contact resistance is given by [12]:

$$R_c = \frac{(R_1 + R_2)}{4} \left(\frac{n \xi H \pi}{F_n} \right)^{\frac{1}{2}} \quad (\Omega) \quad (9)$$

2.2.6 Calculation of convective heat transfer coefficient

The equation of convective heat transfer coefficient, h , is as follows [11]:

$$h = \frac{0.037k}{1} \left(\frac{\rho l V}{\mu} \right)^{0.8} \left(\frac{C_p \mu}{k} \right)^{0.33} \quad (10)$$

where, k is thermal conductivity ($\text{W}\cdot\text{m}^{-1}\cdot\text{°C}^{-1}$); l is relative sliding distance (m); ρ is material density ($\text{kg}\cdot\text{m}^{-3}$); C_p is specific heat ($\text{J}\cdot\text{kg}^{-1}\cdot\text{°C}^{-1}$); μ is friction coefficient; V is relative sliding velocity (m/s).

2.3 Material and experimental parameters

The properties of the three materials are shown in Table 1. In the FE assessment, electric current I was selected to be 150 - 600 A, relative velocities V were selected to be 10km/h - 120 km/h, and normal forces F_n were selected to be 10 N to 290 N in 10N steps. Sliding distances S were selected to be 0 m to 2500m. The friction coefficient μ between upper sample and middle sample was measured as 0.27 [13].

Table 1 Properties of the three materials [14]

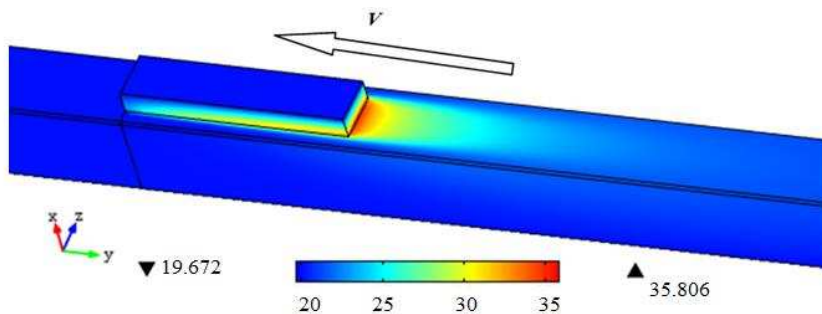
Materials	Resistivity ($\Omega\cdot\text{m}$)	Thermal conductivity ($\text{W}\cdot\text{m}^{-1}\cdot\text{°C}^{-1}$)	Specific heat ($\text{J}\cdot\text{kg}^{-1}\cdot\text{°C}^{-1}$)	Elastic modulus (Pa)	Poisson's ratio	Density ($\text{kg}\cdot\text{m}^{-3}$)	Thermal expansion coefficient ($\times 10^{-6}\cdot\text{°C}^{-1}$)
Stainless steel	0.73 E-6	12.1	502	190 E9	0.3	7930	16
Aluminium	2.9 E-8	238	902	70 E9	0.3	2700	23
Copper impregnated carbon	10 E-6	28	469	12.6 E9	0.425	2400	3.5

3 RESULTS

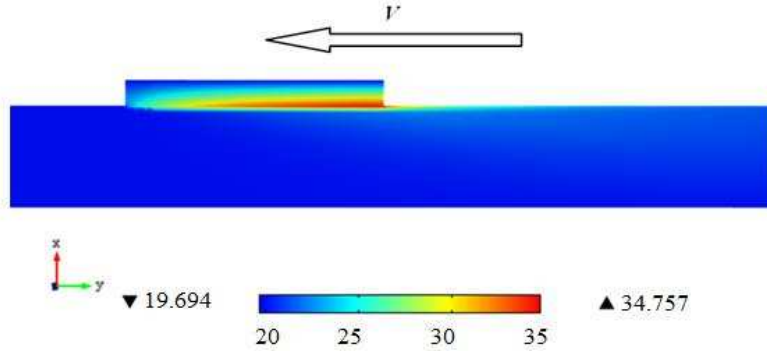
3.1 Influence of electric current on coupled temperature

The temperature distributions of the samples with or without electric current were contrasted respectively in the following finite element simulations: when electric current is 0A or 300 A, normal force 150N, velocity 60 km/h and sliding distance 1500m.

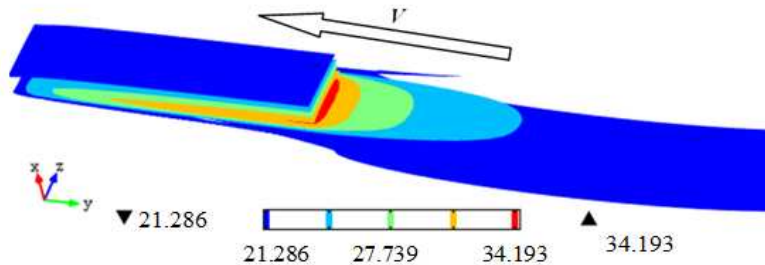
When the normal force is 150 N, relative sliding velocity is 60 km/h, and sliding distance is 1500m without electric current, the resulting temperature distribution contours of friction heat are shown in Figure 4.



(a) 3-D temperature distribution



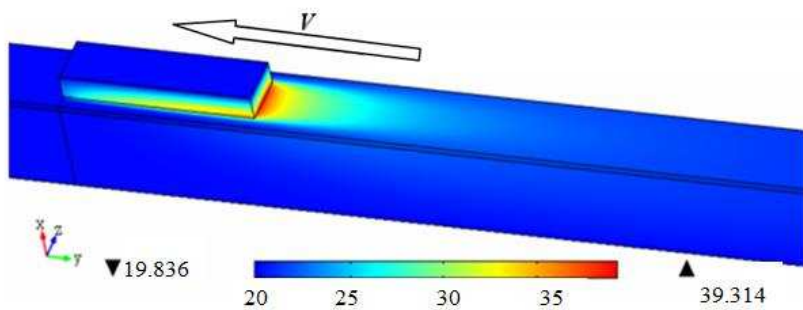
(b) 2-D cross-sectional view of the central axis



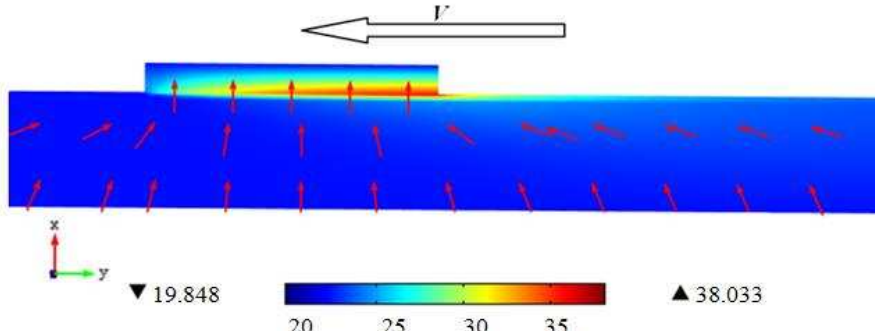
(c) Isothermal layer of frictional heat

Fig. 4 Temperature distribution without current ($I=0$ A, $F_n=150$ N, $V=60$ km/h, $S=1500$ m): (a) 3-D temperature distribution; (b) 2-D cross-sectional view of the central axis; (c) Isothermal layer induced by friction heat; (the white arrow means the collector shoe sliding direction)

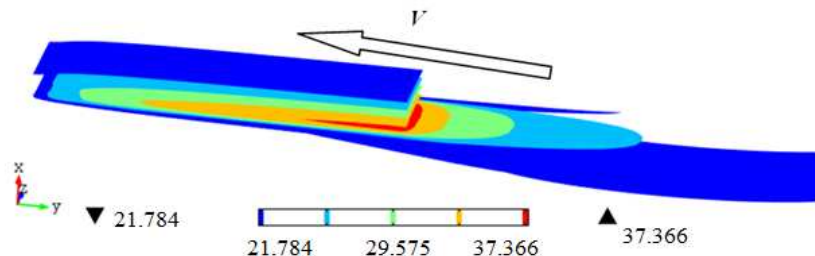
In the 3-D temperature distribution shown in Figure 4(a), the temperature increases from 20.0 °C to 35.8 °C, and the maximum temperature increment is 15.8 °C. In 2-D temperature distribution of cross-sectional view of the central axis in Figure 4(b), the temperature increased from 20.0 °C to 34.8 °C continuously, and the maximum temperature increment was 14.8 °C. In Figure 4(c), the isothermal layer induced by friction heat can be seen clearly and temperature increased discretely in the set condition, and widths of the isothermal layers in third rail are different from each other. The temperature distribution expands around the contact area in a descending tendency, the closer to the electric contact area, the higher the temperature gradient.



(a) 3-D temperature distribution



(b) 2-D cross-sectional view of the central axis



(c) Isothermal layer of coupled heat

Fig. 5 Temperature distribution with electric current ($I=300$ A, $F_n=150$ N, $V=60$ km/h, $S=1500$ m): (a) 3-D temperature distribution; (b) 2-D cross-sectional view of the central axis; (c) Isothermal layer induced by coupled heat;(the white arrow means the collector shoe sliding direction, and the dark arrows in (b) means the flow direction of electric current)

When the electric current is 300 A, normal force 150 N, relative sliding velocity 60 km/h, and sliding distance is 1500 m, the temperature distribution contours of the coupled friction heat and joule heat were shown as in Figure 5. In the 3-D temperature distribution shown in Figure 5(a), the coupled temperature increased from 20.0 °C to 39.3 °C continuously, and the maximum temperature increment was 19.3 °C. In the 2-D temperature distribution shown in Figure 5(b) of the cross-sectional view of the central axis, the temperature is increased from 20.0 °C to 38.0 °C, and the maximum temperature increment is 18.0°C. Current density arrows are shown in Figure 5(b), electric current flows from third rail to collector shoe. In Figure 5(c), the isothermal layer induced by the coupled heat can be seen clearly and temperature increased discretely in the set condition, and widths of the isothermal layers in the third rail are different from each others. The temperature distribution expands around the contact area in a descending tendency, the closer to the electric contact area, the higher the temperature gradients.

Based on the above coupling method applied in 3-D temperature model of Figure 4(a) and Figure 5(a), the maximum coupled temperatures changing with different electric current from 150A to 600A are shown in Figure 6, when the normal force is 150 N, velocity ranges from 10 km/h to 120 km/h and sliding distance is 1500 m. The results show that under constant sliding distance and normal force, the maximum coupled temperature increases with the increasing electric current and sliding velocity as would be expected.

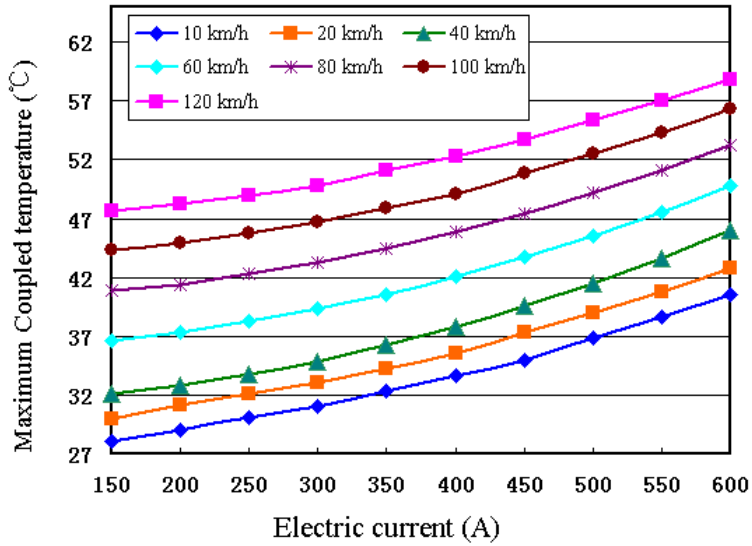


Fig. 6 Variation of maximum coupled temperature with electric current ($F_n=150\text{N}$, $S=1500\text{m}$)

3.2 Influence of normal force on coupled temperature

The variation of maximum coupled temperature changes with normal force from 10 N to 290 N, as shown in Figure 7, when the electric current is 300 A, velocity changes from 10 km/h to 120 km/h and sliding distance is 1500 m. The results show that with constant sliding distance and electric current, the maximum coupled temperature decreases initially then increases with increasing normal force from 10 N to 290 N.

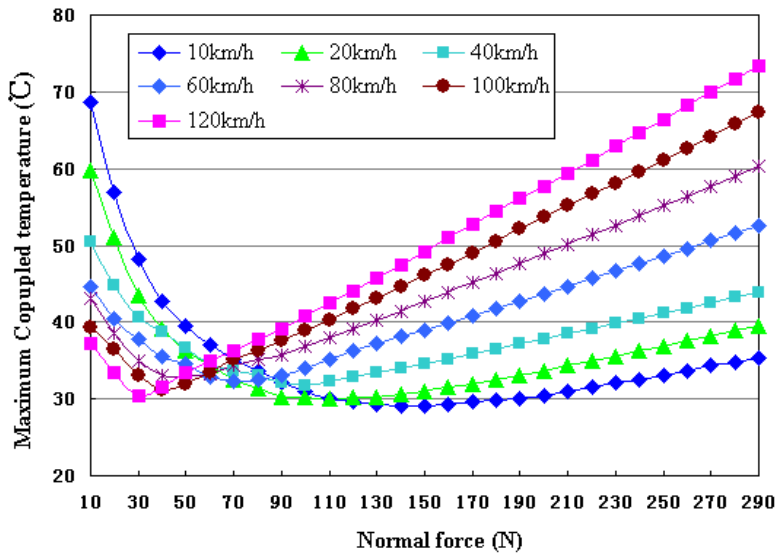


Fig. 7 Variation of maximum coupled temperature with normal force ($I=300\text{ A}$, $S=1500\text{ m}$)

The optimum normal force figure and quadratic polynomial regression equation were gotten in Figure 8, and the optimum normal forces were decreased with increasing of velocities under the constant electric current and sliding distance.

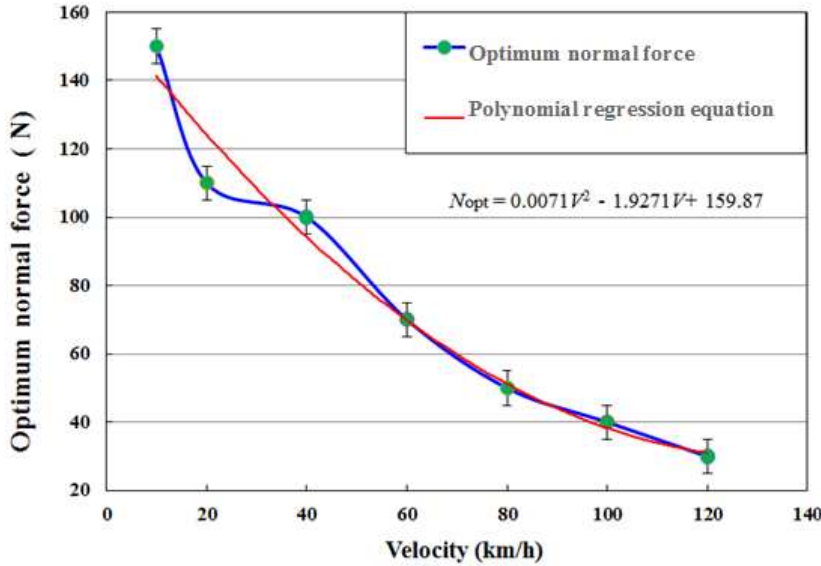


Fig. 8 Variation of optimum normal force with velocity ($I=300$ A, $S=1500$ m)

3.3 Influence of sliding distance on coupled temperature

The variation of maximum coupled temperature with displacement from 0 m to 2500 m is shown in Figure 9, when electric current is from 150A to 600A, normal force 150 N and relative sliding velocity 60km/h. Under the same sliding distance, the greater the current is, the greater the maximum coupled temperature is. The maximum coupled temperature increases initially then gradually becomes stable with an increase of sliding distance. When each sliding distance was larger than 1500 m, all the maximum coupled temperatures were in a stable condition. In previous coupled temperature calculations (Figure 4, Figure 5, Figure 6 and Figure 7), the sliding distances were all selected to be 1500m.

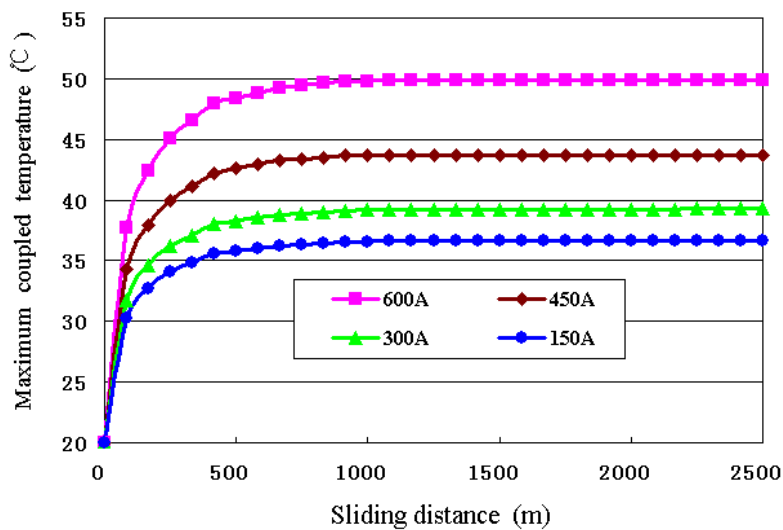
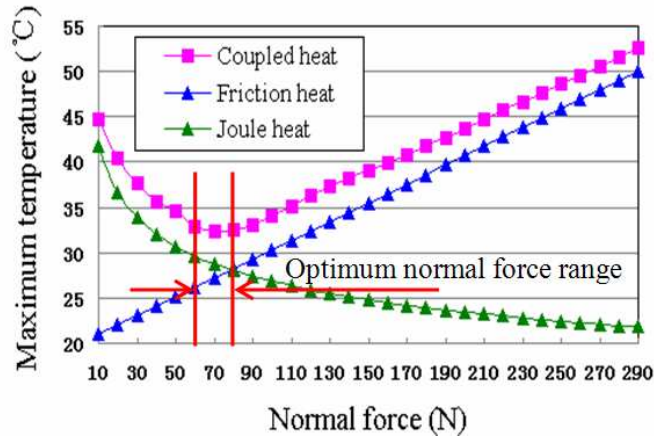


Fig. 9 Variation of maximum coupled temperature with displacement ($F_n=150$ N, $V=60$ km/h)

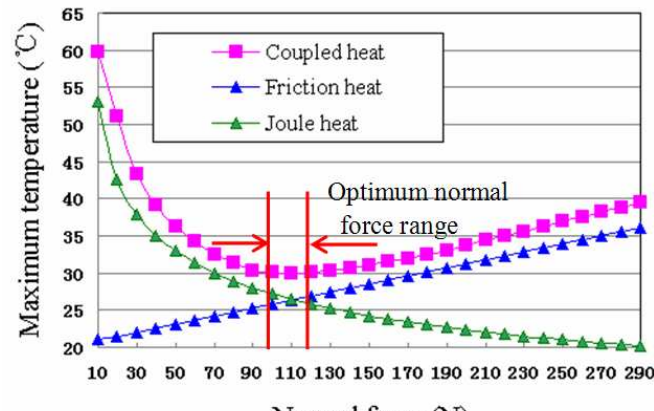
The regulation of maximum coupled temperature changing with sliding distance is consistent with the results of experimental work [9].

4 DISCUSSION

In Figure 6, with 1500 m sliding displacement and 150 N normal force, the friction heat Q_f sourced from sliding friction power is a constant (see Equation 3). But the joule heat Q_j increases with an increase of electric current (see Equation 5), so the maximum coupled temperature increases with an increase of electric current as shown in Figure 6.



(a)



(b)

Fig. 10 Variation of maximum temperature with normal force ($I=300$ A, $S=1500$ m): (a) $V=60$ km/h (b) $V=20$ km/h

Under different normal force, maximum temperature induced by the coupled heat, friction heat or joule heat are shown in Figure 10. Figure 10 has the same working parameters as the data in Figure 7. The maximum temperature induced by coupled heat in Figure 10 is the maximum coupled temperature in Figure 7. Figure 10(a) is with a velocity of 60 km/h and Figure 10 (b) is with a velocity 20 km/h. In Figure 10 (a), the maximum temperatures induced by joule heat decrease with increasing normal force, because the increased normal force makes the contact resistance R_c decrease (see Equation 9) and joule heat Q_r decrease (see Equation 5). The maximum temperature induced by friction heat increases with the increasing normal force, because the increased normal force makes the mechanical friction heat Q_f increase (see Equation 3). The maximum coupled temperature is induced by coupled heat of joule heat and friction heat. Figure 10(b) has the same changing regulation with Figure 10(a).

In the process of friction and wear with electric current, the total heat is the coupled result of mechanical friction heat and joule heat, while arcs do not occur. The two kinds of heat are competitive with each other. When normal force is less, the contact resistance heat becomes the main heat source, but when normal force is greater, mechanical friction heat becomes the main heat source. So the maximum coupled temperature decreases initially then increases with increasing normal force (see Figure 7 and Figure 10). An optimum normal force range exists in a current-carrying tribological system, where the maximum coupled temperature is at its lowest value (see Figure 7 and Figure 10). In Figure 10(a), when velocity is 60km/h, this optimum normal force range is between 60 N and 80 N. In Figure 10(b), and when velocity is 20 km/h, this optimum normal force range is between 100 N and 120 N.

In Figure 9, under constant 60 km/h velocity and 150 N normal force, the mechanical friction heat Q_f increases with increasing sliding distance (see Equation 3), but the convective heat transfer coefficient increases with increasing sliding distance (see Equation 10). When the generation of heat is balanced to the loss of heat, the maximum coupled temperature becomes stable. Joule heat Q_e increases with increasing electric current (see Equation 5). So each maximum coupled temperature increases initially then gradually becomes stable with increasing sliding distance, and stabilized maximum coupled temperature increase with increasing electric current.

5 CONCLUSIONS

The main conclusions drawn from finite element assessment of the temperature field couple under joule heat and friction heat in a collector/third rail contact may be summarized as follows:

1. A finite element couple method has been developed for the temperature rise and temperature field assessment of collector/third rail under friction and wear with electric current. **The joule heat module in COMSOL Multiphysics 4.3b is the dominant work mode, and friction heat was coupled in the joule heat module by friction work.**
2. Under different relative velocities, the maximum coupled temperature increases with an increase of the electric current.
3. The maximum coupled temperature increases initially then gradually becomes stable with an increase of sliding distance.
4. The maximum coupled temperature initially decreases then increases with increasing normal force, and an optimum normal force range exists and can be calculated. Working under the optimum normal force zone, the maximum coupled temperature is lowest.

For the control of temperature rise in actual working conditions, finite element should be an important method for assessment, and it will be meaningful in control of the wear volume losses in the process of friction and wear with electric current.

ACKNOWLEDGEMENTS

The authors would gratefully thank for the National Natural Science Fund of China (No.51005188), the Youth Science and Technology Fund of Sichuan Province (No.2011JQ0039), the Talent Fund of Xihua University (No.R0920203), and the Science and Technology Fund of Ministry of Human Resources and Social Security of the P.R. China

(2013), Key Scientific Research Fund of Education Department in Sichuan Province (No. 13ZA0021).

REFERENCES

- 1 **He, D.H., Manory, R., Sinkis H.** A sliding wear tester for overhead wires and current collectors in light rail systems. Wear 2000; **239**(1): 10-20.
- 2 **Nagasawa, H., Kato, K.** Wear mechanism of copper alloy wire sliding against iron-base strip under electric current. Wear 1998; **216**(2): 179-183.
- 3 **Zhao, H., Barber, G.C., Liu, J.** Friction and wear in high speed sliding with and without electrical current. Wear 2001; **249**(5-6): 409-414.
- 4 **Zaidi, H., Csapo, E., Nery, H., Paulmier, D.** Friction coefficient variation in a graphite-graphite dynamical contact crossed by an electric current. Surf Coat Technol 1993; **62**(1-3): 388-392.
- 5 **Dong, L., Chen, G.X., Zhu, M.H., Zhou, Z.R.** Wear mechanism of aluminium-stainless steel composite conductor rail sliding against collector shoe with electric current. Wear 2007; **263**(1-6): 598-603.
- 6 **Zheng, R.G., Zhan, Z.J., Wang, W.K.** Wear behavior of Cu-La₂O₃ composite with or without electrical current. Wear 2010; **268**(1-2): 72-76.
- 7 **Argibay, N., Bares, J.A., Sawyer, W.G.** Asymmetric wear behavior of self-mated copper fiber brush and slip-ring sliding electrical contacts in a humid carbon dioxide environment. Wear 2010; **268**(3-4): 455-463.
- 8 **Chen, G.X., Li, F.X., Dong, L., Zhu, M.H., Zhou, Z.R.** Friction and wear behaviour of stainless steel rubbing against copper-impregnated metallized carbon. Tribol Int 2009; **42**(6): 934-939.
- 9 **Ding, T., Chen, G.X., Bu, J., Zhang, W.H.** Effect of temperature and arc discharge on friction and wear behaviours of carbon strip/copper contact wire in pantograph-catenary systems. Wear 2011; **271**:1629-1636.
- 10 **Gerhard, M.** Composite conductor rail of aluminum and steel, in particular high-performance railway conductor rail. Patent 5061829, USA, 1991.
- 11 **Song, M., Kovacevic, R.** Thermal modeling of friction stir welding in a moving coordinate system and its validation. Int J Mach Tool Manuf 2003, **43**(6): 605-615.
- 12 **Holm, R.** Electric contacts theory and application. Berlin: Springer, 1967, p.76.
- 13 **Dong, L., Chen, G.X., Zhu, M.H., Zhou, Z.R.** Tribological characteristics between third rail and collector shoe under electric current. Tribology 2007; **27**(3): 274-278.
- 14 **Da, S.F.M.** Electrical contact materials manual. Beijing: Mechanical Industry Press, 1987, p.116.

APPENDIX

Notation

A_c	total electric contact area (m^2)
A_r	real contact area (m^2)
A_s	area of single contact point area (m^2)
C_p	specific heat ($\text{J}\cdot\text{kg}^{-1}\cdot\text{°C}^{-1}$)
E_{cf}	energy conversion factor
F_n	normal force (N)
h	convective heat transfer coefficient
H	hardness (MPa)
I	electric current (A)
k	thermal conductivity of material ($\text{W}\cdot\text{m}^{-1}\cdot\text{°C}^{-1}$)
l	relative sliding distance (m)
N_{opt}	optimum normal force (N)
Q	power produced by heat (W)
Q_f	mechanical friction heat (J)
\dot{Q}_f	friction heat flux ($\text{W}\cdot\text{m}^{-2}$)
Q_j	joule heat (J)
\dot{Q}_j	joule heat flux ($\text{W}\cdot\text{m}^{-2}$)
r	outer normal direction of the object boundary
R_l	resistivity of collector shoe ($\Omega\cdot\text{m}$)
R_2	resistivity of third rail contact surface ($\Omega\cdot\text{m}$)
R_c	electric contact resistance (Ω)
R_{c1}	contraction resistance of collector shoe (Ω)
R_{c2}	contraction resistance of third rail contact surface (Ω)
t	relative sliding time (s)
T	temperature (K)
T_0	initial node temperature (K)
V	relative sliding velocity (m/s)
α	radius of actual contact surface (m)

μ friction coefficient

ρ material density ($\text{kg}\cdot\text{m}^{-3}$)

